Electrochemical behavior of palladium modified amino-functionalized macroporous copolymer

Bojana M. Marković, Danijela D. Maksin, Zorica D. Mojović, Zorica M. Vuković, Aleksandra B. Nastasović, Dušan M. Jovanović

PII: S1572-6657(17)30020-6
DOI: doi: 10.1016/j.jelechem.2017.01.018
Reference: JEAC 3065

To appear in: *Journal of Electroanalytical Chemistry*

Received date: 18 October 2016
Revised date: 26 December 2016
Accepted date: 7 January 2017

Please cite this article as: Bojana M. Marković, Danijela D. Maksin, Zorica D. Mojović, Zorica M. Vuković, Aleksandra B. Nastasović, Dušan M. Jovanović , Electrochemical behavior of palladium modified amino-functionalized macroporous copolymer. The address for the corresponding author was captured as affiliation for all authors. Please check if appropriate. Jeac(2017), doi: 10.1016/j.jelechem.2017.01.018

Electrochemical behavior of palladium modified amino-functionalized macroporous copolymer

Bojana M. Marković[a], Danijela D. Maksin[b], Zorica D. Mojović[c*], Zorica M. Vuković[c], Aleksandra B. Nastasović[a], Dušan M. Jovanović[c]

[a]*University of Belgrade, Institute of Chemistry, Technology and Metallurgy, Department of Chemistry, Njegoševa 12, 11000 Belgrade, Republic of Serbia*

[b]*University of Belgrade, Vinča Institute of Nuclear Sciences, P.O. Box 522, 11001 Belgrade, Republic of Serbia*

[c]*University of Belgrade, Institute of Chemistry, Technology and Metallurgy, Department of Catalysis and Chemical Engineering, Njegoševa 12, 11000 Belgrade, Republic of Serbia*

[*]Corresponding Author: Zorica D. Mojović, Ph.D.

e-mail address: zoricam@nanosys.ihtm.bg.ac.rs

tel.: +381 11 2630213

fax.: +381 11 2637977

Abstract

In this study, macroporous poly(glycidyl methacrylate-*co*-ethylene glycol dimethacrylate) was synthesized by suspension copolymerization, functionalized by ring-opening reaction of the pendant epoxy groups with diethylene triamine and used for immobilization of Pd(II) ions from chloride and nitrate solutions under batch experimental condition. The amino-functionalized sample and samples with immobilized Pd(II) ions were characterized by Fourier transform infrared spectroscopy (FTIR) analysis and scanning energy-dispersive X-ray spectroscopy (SEM-EDX). The electrochemical behavior of electrodes composed of synthesized samples was tested in 0.1 M H_2SO_4 by means of cyclic voltammetry (CV). The shape of recorded CV showed dependence on the type of Pd-salt used for Pd immobilization. The reaction of oxidation of 4-chlorophenol (4-CP) from 0.1 M H_2SO_4 at investigated samples was also studied. Electrooxidation of 4-CP resulted in passivation and formation of reversible hydroquinone/benzoquinone on both investigated electrodes, although hydroquinone/benzoquinone formation was more pronounced on Pd immobilized from nitrite solution.

Key words: PGME, palladium, chlorophenol, electrooxidation

1. Introduction

The great number of papers reports the findings regarding electrochemical behavior of polycrystalline [1], monocrystalline [2,3] and nanostructured [4,5] Pd electrodes. Palladium – polymer combined films were investigated for various applications, like reduction of dissolved oxygen in water and the reduction of nitrobenzene to aniline [6], hydrogenation of unsaturated alcohols [7], the oxygen reduction reaction (ORR) and detection of As (III) [8], as "dip catalyst" for the Suzuki–Miyaura reaction [9], biosensors [10], etc.

The conductive polymers such as polyaniline and polypyrrole are usually employed in the investigation. In that manner the polymer contributes to the electrochemical response of the investigated composite material. Amino-functionalized poly(glycidyl methacrylate-*co*-ethylene glycol dimethacrylate) (PGME) has ability to absorb heavy metals (Cu(II)) [11], Cr(VI) [12,13], Mo(VI) [14], Tc(VII) [15], depending on pH through several mechanisms, such as chelation, electrostatic interactions or ion exchange [16]. In this manner palladium cluster of nanometer dimensions can be formed on PGME. Since PGME is non-conductive polymer the electrochemical behavior of solely nano-sized palladium particles can be assessed. In this work palladium nanoparticles were deposited on macroporous PGME copolymer functionalized with diethylene triamine, PGME 20/14-deta. The aim of this paper was to investigate the influence of anion of palladium salt on the properties of formed palladium deposit on PGME 20/14. The electrochemical properties of synthesized materials were investigated from acidic solution. The electrocatalytic properties of palladium modified PGME 20/14 were tested in the electrooxidation of 4-chlorophenol. The electrooxidation of chlorophenol is a complex process. The oxidation of chlorophenols proceeds through oxidation of hydroxyl group producing phenoxy radical. Phenoxy radical can undergo dimerization or polymerization with other phenoxy radical or unreacted chlorophenol molecules forming oligomers or polymerized film. The presence of the later on the electrode surface causes fouling of the electrode or its complete passivation. More favorable pathway with lower polymerization rate is a formation of soluble hydroquinones/quinones from phenoxy radical [17–19]. Palladium oxide is expected to act as catalyst for anodic reaction involving simple organic compounds [20–23]. The investigation of electrochemical reaction of benzoic acid on palladium showed that palladium does not favor irreversibly adsorbed species [22]. On the other hand, the electrocatalytic properties of palladium oxides are influenced by the oxide composition that is strongly dependent on the experimental conditions [23].

2. Experimental

2.1. Materials

All the chemicals used for copolymer synthesis were analytical grade products and used as received. Glycidyl methacrylate, diethylene triamine, 2,2'-azobisiso-butyronitrile (AIBN), cyclohexanol and tetradecanol were purchased from Merck (Germany). Ethylene glycol dimethacrylate was obtained from Sigma-Aldrich (Germany). Poly(N-vinyl pyrrolidone) (PVP, Kollidone 90) was purchased from BASF (Germany). Reagents used for electrochemical experiments were of analytical grade and were used without further purification. Metal solutions were prepared from reagent grade $Pd(NO_3)_2$ (Merck, Germany) and $PdCl_2$ (Sigma-Aldrich) using deionized water (Milli-Q Millipore, 18 $M\Omega cm^{-1}$ conductivity).

2.2. Characterization

Fourier transform infrared (FTIR) spectra were recorded using a Nicolet 380 spectrometer equipped with a Smart Orbit^{TM} ATR attachment containing a single-reflection diamond crystal. Pore size distributions were determined by a high pressure mercury intrusion porosimeter Carlo Erba Porosimeter 2000 (Washington, USA, software Milestone 200), operating in the interval from 0.1 to 200 MPa. The samples were previously degassed at room temperature and pressure of 0.5 kPa. The energy dispersive spectroscopic (EDS) analysis was performed on JEOL JSM 5800 instrument operating at 20kV.

2.3. PGME 20/14 preparation, functionalization with diethylene triamine and immobilization of Pd(II) ions

Macroporous crosslinked copolymer PGME 20/14 was obtained by radical suspension copolymerization of glycidyl methacrylate (GMA) and ethylene glycol dimethacrylate (EGDMA) as crosslinker in the presence of inert component, i.e. binary mixture of cyclohexanol and tetradecanol as previously described [24]. The fraction of particles with average particle diameter less than 100 μm was used for functionalization with diethylene triamine using the procedure described elsewhere [25] and labeled as PGME 20/14-deta. In the sample label the letter P designates polymer, GM stands for glycidyl methacrylate (GMA) while E stands for ethylene glycol dimethacrylate (EGDMA). The first number in a sample label stands for the share of tetradecanol in the inert component (w/w) and the second one for

the number of C-atoms (14 for tetradecanol). The additional label -deta designates sample functionalized with diethylene triamine.

Pd(II) ions were immobilized on PGME 20/14-deta from $PdCl_2$ and $Pd(NO_3)_2$ solutions (C_i=1000 ppm). The samples were labeled as PGME 20/14-deta/$PdCl_2$ and PGME 20/14-deta/$Pd(NO_3)_2$.

2.4. Electrochemical experiment

In order to use the investigated materials as electrode materials, the samples were homogeneously dispersed in original Nafion solution using an ultrasonic bath (Ultrasons-H, J.P. Selecta). Droplets (10μl) of these suspensions were placed on the surface of a glassy carbon electrode (GCE) (area = 0.0314 cm^2). After solvent evaporation, the sample was uniformly distributed on the GCE in the form of a thin layer. For the electrochemical investigations in a three-electrode glass cell, the modified GCE was used as working electrode. The reference electrode was Ag/AgCl in 3 M KCl, while a platinum foil served as a counter electrode. The electrochemical behavior of samples was investigated from 0.1 M H_2SO_4 supporting solution by cyclic voltammetry. 4-chlorophenol (4-CP) oxidation was investigated for starting concentration of 4-CP of 5mM in 0.1 M H2SO4.The device used for the electrochemical measurements was 797 VA Computrace Metrohm. Cyclic voltammograms have been recorded at the scan rate of 50 mV s^{-1}. Starting potential for all measurements was lower cathodic limit of recorded potential range. Linear voltammetry for Tafel analysis was recorded at scan rate of 10 mV s^{-1}.

3. Results and discussion

3.1. FTIR analysis

The FTIR spectra of the amino-functionalized PGME sample and samples with immobilized Pd(II) ions were recorded and presented in Fig. 1.

Figure 1.

The bands for ester vibrations at ~1720 cm^{-1}($\nu_{C=O}$), as well as the bands at ~ 2850 cm^{-1}($\nu_{C-H\ sym}$), 2950 cm^{-1} ($\nu_{C-H\ asym}$), 1455 cm^{-1} (δ_{CH2}) and 1160 cm^{-1} (ν_{C-O-C}) are present in PGME 20/14-deta spectra. The wide band at ~3050-3700 cm^{-1}(ν_{N-H}+ ν_{O-H}), the bands at ~1260 cm^{-1}(ν_{C-N}), ~1560 cm^{-1} and 1650 cm^{-1} (δ_{NH}, δ_{NH2}), as well as the band at ~1390 cm^{-1} (ν_{NH}) indicate the presence of -NH and -NH_2 groups in PGME 20/14-deta as a result of functionalization with diethylenetriamine. The band at ~3050-3700 cm^{-1} appeared also in the

spectra of samples with immobilized Pd(II) ions. The peaks at 3240 cm^{-1} for PGME 20/14-deta/$PdCl_2$ and 3230 cm^{-1} for PGME 20/14-deta/$Pd(NO_3)_2$ appeared partly because of the presence of -OH groups after functionalization with amines and/or due to hydrogen bonds. The peak at 3350 cm^{-1}($\nu_{O\text{-}H}$) was shifted to 3460 cm^{-1} for PGME 20/14-deta/$PdCl_2$ and 3470 cm^{-1} for PGME 20/14-deta/$Pd(NO_3)_2$, possibly due to the coordination of Pd(II) ions with water and/or OH- ions. In PGME 20/14-deta/$PdCl_2$ and PGME 20/14-deta/$Pd(NO_3)_2$ spectra the band at ~1560 cm^{-1} (δ_{NH}) disappeared, while the δ_{NH2} peak was shifted to 1640 cm^{-1}, indicating the Pd(II) binding to PGME 20/14-deta [26]. According to Golcuk et al. the binding with the metal alters the hybridization type around nitrogen causing the weakening of NH bond [27].

Another evidence for Pd(II) binding is the appearance of the wide band at 530 cm^{-1} for PGME 20/14-deta/$Pd(NO_3)_2$ and 511 cm^{-1} for PGME 20/14-deta/$PdCl_2$. Namely, the peak for $\nu_{Pd\text{-}N}$ appears in the frequency range 528-436 cm^{-1}, depending on the nature of the ligands in the complex [28].

3.2. Porosity

The cumulative and differential pore size distribution curves for PGME 20/14-deta as well as for samples with immobilized Pd(II) ions, i.e. for PGME 20/14-deta and PGME 20/14-deta/$Pd(NO_3)_2$ were determined by mercury porosimetry. For the sake of clarity, only the pore size distribution curves for PGME 20/14-deta and PGME 20/14-deta/$Pd(NO_3)_2$ were given in Figure 2. The curve for PGME 20/14-deta/$PdCl_2$ was omitted since it almost overlaps with PGME 20/14-deta/$Pd(NO_3)_2$ curve. The porosity parameters of investigated samples (specific pore volume, V_s, specific surface area, S_{Hg}, and pore diameter which corresponds to half of pore volume, $D_{V/2}$) calculated from the cumulative pore volume distribution curves as described in the literature [29] are presented in Table 1.

Figure 2.

Table 1.

As seen from Fig. 2, cumulative pore size distribution curves for PGME 20/14-deta and PGME 20/14-deta/$Pd(NO_3)_2$ have an inverse S shape with a clearly defined inflection points. The calculated porosity parameters confirm the predominant macroporous structure of PGME 20/14-deta ($D_{V/2}$ > 50 nm). Also, the constant increase in mesoporous area instead of a plateau observed in the area of mesopores (pore diameter <50 nm) suggests the presence of smaller mesopores and micropores. The Pd(II) immobilization caused a shift in the pore size

for PGME 20/14-deta/$PdCl_2$ and PGME 20/14-deta/$Pd(NO_3)_2$ towards larger pores, which led to the slight decrease in the specific surface area. On the other hand, the porosity parameters for PGME 20/14-deta/$PdCl_2$ negligibly differ from the data for PGME 20/14-deta/$Pd(NO_3)_2$.

3.3. SEM-EDS analysis

The surface and cross-section morphology of the amino-functionalized PGME 20/14 sample and samples with immobilized Pd(II) ions was examined by SEM-EDS (energy-dispersive X-ray spectroscopy) analysis. The results are presented in Fig. 3 and Table 2.

Figure 3.

As seen from Fig. 3, PGME 20/14-deta particles have regular spherical shape and porous morphology which was retained after the immobilization of Pd(II) ions (samples PGME 20/14-deta/$Pd(NO_3)_2$ and PGME 20/14-deta/$PdCl_2$). The micrographs of the particles surface display a dense and porous surface texture. Also, the immobilization of Pd(II) ions resulted in the formation of discrete bright aggregates deposited on the macroporous support surface (Fig. 3e and Fig. 3h). The SEM micrographs of the particles cross-sections (Fig. 3c, Fig. 3f and Fig. 3i) show highly developed internal porous structure composed of a large number of globules and interconnected with channels and pores.

The SEM-EDS analysis enabled investigation of the elements distribution before and after immobilization of Pd(II) ions at a depth of 100–1000 nm from the surface. Qualitative SEM-EDS analysis confirmed the presence of all expected elements for PGME 20/14-deta (C, O and N) as well as for PGME 20/14-deta/$PdCl_2$ and PGME 20/14-deta/$Pd(NO_3)_2$ (C, O, N and Pd). Additionally, the presence of Cl was observed in the sample PGME 20/14-deta/$PdCl_2$.

Table 2.

The results given in Table 2 provide a quantitative view of the elemental composition in the inspection field in both mass and atomic percent. The C/O and N/C atomic ratios have been calculated for the surface and cross section of PGME 20/14-deta particles for comparison. The C/O atomic ratios in the surface and cross section were approximately 7.85 and 5.31, respectively. The N/C atomic ratios in the surface and cross section were approximately 0.209 and 0.198, respectively. These small differences could be the consequence of the fact that some epoxy groups in macroporous PGME copolymer usually remain inside the crosslinked copolymer, not being accessible for subsequent reaction with diethylene triamine [30]. EDS analysis proved that a significant amount of palladium was bonded to the active

sites on the interior surface of the particles as well as on the exterior denoting the possibility of palladium diffusion through the porous structure of amino-functionalized macroporous PGME 20/14-deta. The higher amount of Pd sorbed both on the particle surface and cross section was observed for PGME 20/14-deta/$PdCl_2$. Also, Pd was evenly distributed on the surface and cross section of the sample PGME 20/14-deta/$PdCl_2$, unlike the sample PGME 20/14-deta/$Pd(NO_3)_2$ for which twice more Pd was sorbed on the surface than in cross section Additionally, SEM-EDS spectra at gray and bright areas on the surface of samples PGME 20/14-deta/$PdCl_2$ and PGME 20/14-deta/$Pd(NO_3)_2$ were collected. Analyzed areas were marked blue (Fig. 4).

Figure 4.

Detailed analysis of bright and gray areas on the surface of the PGME 20/14-deta/$PdCl_2$ and PGME 20/14-deta/$Pd(NO_3)_2$ particles confirmed the presence of Pd in discrete bright aggregates.

3.4. Electrochemical behavior

The electrochemical behavior of PGME 20/14-deta/$PdCl_2$ and PGME 20/14-deta/$Pd(NO_3)_2$ was tested in 0.1 M H_2SO_4. It can be seen that electrochemical response at scan rate of 10 mVs^{-1} was different for these two samples (Fig. 5).

Figure 5.

Higher currents were recorded for GCE modified with PGME 20/14-deta/$Pd(NO_3)_2$ sample. Cyclic voltammograms of both samples exhibited peak (Ia) at 0.435 V *vs.* Ag/AgCl electrode (inset in Fig. 5). CV of PGME 20/14-deta/ $PdCl_2$ exhibited another anodic peak (IIa) at 0.650 V. Cathodic peak (Ic), although poorly resolved, was recorded at potential of 0.355 V at CV for both samples. CV of PGME 20/14-deta/$Pd(NO_3)_2$ exhibited another anodic peak (IIIa) at 0.820 V and cathodic peak (IIc) at 0.215 V. The onset potential for oxygen evolution reaction (OER) for both samples was at approximatelly1.0 V. The onset potential for hydrogen evolution reaction (HER) was at 0.02 V and 0.07 V for PGME 20/14-deta/$PdCl_2$ and PGME 20/14-deta/$Pd(NO_3)_2$, respectively. Currents of OER and HER for PGME 20/14-deta/$Pd(NO_3)_2$ were higher than for PGME 20/14-deta/$PdCl_2$ indicating that PGME 20/14-deta/$Pd(NO_3)_2$ was electrocatalytically more active.

The shape of CV profiles in the potential range of the oxide growth is greatly influenced by the surface structure of Pd electrodes [31]. The influence of anodic potential limit on the

shape of the cyclic voltammogram was studied (Fig. 6a and Fig. 6b) in order to assign peaks to specific reactions on the electrode surface.

Figure 6.

It was noted that peaks Ia and Ic appeared when recording was performed in narrow potential range when the anodic limit was 0.5V. It was also observed that peak Ic was shifted towards more negative values with the increase of anodic potential limit until peaks Ic and IIc were obtained. Peak Ic was poorly resolved for CV of both samples, while well-defined peak IIc was obtained only for PGME 20/14-deta/$Pd(NO_3)_2$. The peak Ia can probably be ascribed to the oxide formation at very small palladium particles. Similar increase in double layer region was noted by Salvador-Pascual et al. [32] at the voltammogram of the palladium electrode with the synthesized nanoparticles and associated this behavior to the particle size. In the line with this conclusion is the fact that standard electrochemical behavior for hydrogen absorption-desorption on and into palladium in acidic solutions was not observed. Possible assignment to peak IIa is a dissolution of palladium [33], probably due to the presence of Cl^- ions adsorbed by PGME 20/14-deta which could promote solvation process of palladium. Namely, palladium dissolution is more likely to occur in the presence of Cl^- and I^- ions in solution than in the presence of SO_4^- ions [34]. Oxide reformation currents did not overlap in the same potential range during consecutive forward sweeps for both investigated samples. This might indicate that the dissolution of Pd took place at higher anodic potentials. This feature was accompanied by the increase of peak current at potential of Ia ascribed to oxidation of small palladium particles. It can be assumed that dissolved palladium might stay in the vicinity of the electrode surface and can be deposited in consecutive positive sweep [35]. The peak IIIa recorded for PGME 20/14-deta/$Pd(NO_3)_2$ sample corresponds to the oxide formation at the terrace atomic rows [31], while the peak IIc corresponds to the reduction of this oxide. The inserted pictures in Fig. 6a and Fig. 6b represent ten repetitive cyclic voltammograms recorded in full investigated potential range. Similar processes were noted to occur at cyclic voltammograms recorded by repetitive cycling as well as by changing of anodic potential limit. In both cases the changes are more visible at PGME 20/14-deta/$Pd(NO_3)_2$ electrode.

According to SEM-EDS analysis more palladium was present in PGME 20/14-deta/$PdCl_2$ sample but higher currents were obtained for PGME 20/14-deta/$Pd(NO_3)_2$. Furthermore, the amount of palladium on the surface and inside of the particle of PGME 20/14-deta/$PdCl_2$ was almost the same, while the amount of surface palladium in PGME

20/14-deta/$Pd(NO_3)_2$ sample was almost two times higher than the amount of palladium inside particle. Higher current obtained for PGME 20/14-deta/$Pd(NO_3)_2$ can be explained in terms of higher surface area of deposited palladium.

The process of 4-chlorophenol oxidation was tested on investigated electrodes. The electrodes were cycled in 4-CP free 0.1 M H_2SO_4 solution in the potential range from -0.3 V to +1.5 V in order to enable formation of palladium oxides. After that electrodes were transferred to acidic solution with 4-CP and cycled in the same potential range. Successive ten cycles for PGME 20/14-deta/$PdCl_2$ and PGME 20/14-deta/$Pd(NO_3)_2$ in 4-CP containing solution are presented in Fig. 7a and Fig. 7b, respectively. The electrochemical response was similar for both tested electrodes. In the first cycle the oxidation peak at 1.0 V appeared at the foot of oxygen evolution reaction. This peak corresponds to the oxidation of hydroxyl group of 4-CP. The oxidation products, such as hidroquinone and catechol, as well as phenoxy radicals are formed during this oxidation. The hidroquinone and catechol are reduced during cathodic sweep that is recorded at CV as current rise at potential range 0.15 V - 0.55 V. In the second cycle new peaks appeared at 0.43 and 0.55 V corresponding to reoxidation of these species. For phenol these pairs of peaks correspond to hydroquinone/p-benzoquinone and catechol/o-benzoquinone redox couples. For 4-CP the formation of chlorinated or non-chlorinated hydroquinone/benzoquinone is expected. The potential of these peaks overlaps with formation of palladium oxide on small palladium particles.

Figure 7.

However, electrodes showed different behavior toward passivation effect. The current increase during first six cycles for PGME 20/14-deta/$PdCl_2$ was observed. Further cycling lead to a current decrease due passivation. Phenoxy radicals formed at high anodic potential polymerized and formed strongly adherent film. For PGME 20/14-deta/$Pd(NO_3)_2$ current increased during all ten recorded cycles. The highest achieved currents were similar for both electrodes. It can be concluded that reaction rate of 4-CP oxidation on PGME 20/14-deta/$PdCl_2$ was higher than on PGME 20/14-deta/$Pd(NO_3)_2$.

Further testing was performed in 4-CP containing acidic solution without previous conditioning of the electrodes in 4-CP free solution (Fig. 8). The same processes were noted. The obtained currents were lower than for the electrode previously conditioned in acidic solution. For PGME 20/14-deta/$PdCl_2$ all processes were shifted toward more positive potentials.

Figure 7.

The Tafel plots for CP oxidation at a modified GC electrode obtained after the measured currents were corrected for diffusion to give the kinetic currents in the mixed activation-diffusion region (Fig. 9). The values of Tafel slopes amounted 115 mV dec^{-1} and 110 mV dec^{-1} for PGME 20/14-deta/$PdCl_2$ and PGME 20/14-deta/$Pd(NO_3)_2$, respectively, after cycling in 0.1 M H_2SO_4 prior phenol oxidation. The values of Tafel slopes obtained without previous cycling amounted 148 mV dec^{-1} and 130 mV dec^{-1} for PGME 20/14-deta/$PdCl_2$ and PGME 20/14-deta/$Pd(NO_3)_2$, respectively. The Tafel slope of 118 mV dec^{-1}, corresponding to the first charge transfer as rate-determining step, is expected according to the literature [18,19]. The higher values of obtained Tafel slopes indicate complex mechanism, probably formation of palladium oxide occurring simultaneously with phenol oxidation.

Figure 9.

Higher oxidation rate of 4-CP, as well as passivation rate were obtained for PGME 20/14-deta/$PdCl_2$ than for PGME 20/14-deta/$Pd(NO_3)_2$. The current ratio of 4-CP oxidation and reversible couple oxido-reduction is higher for PGME 20/14-deta/$PdCl_2$, than for PGME 20/14-deta/$PdC(NO_3)_2$. This might indicate that different 4-CP oxidation paths were favored on investigated electrodes, probably as the consequence of different shape of palladium nanoparticles, i.e. different position of palladium active centers on the step or terrace as suggested in literature [36–38].

The results in this study show that palladium (nano) particles with electrocatalytic activity could be obtained by a simple method. Also, the choice of the anion affects the formation of different palladium structures, which results in a different electrocatalytic activity for the oxidation of 4-CP.

4. Conclusion

Macroporous poly(glycidyl methacrylate-*co*-ethylene glycol dimethacrylate) was synthesized by suspension copolymerization, functionalized by ring-opening reaction of the pendant epoxy groups with diethylene triamine and used for immobilization of Pd(II) ions from chloride and nitrate solutions under batch experimental condition (samples PGME 20/14-deta/$PdCl_2$ and PGME 20/14-deta/$Pd(NO_3)_2$). The FTIR analysis confirmed functionalization of PGME 20/14 and successful Pd binding. The shape of the cumulative pore size distribution curve cumulative pore size distribution curve and calculated porosity parameters confirm the predominant macroporous structure of PGME 20/14-deta. Also, the constant increase in mesoporous area instead of a plateau in the area of mesopores suggests

the presence of smaller mesopores and micropores. SEM-EDS suggests that the immobilization of Pd(II) ions did not affect the regular spherical shape and porous morphology of PGME 20/14-deta. The immobilization of Pd(II) ions resulted in the formation of discrete bright aggregates deposited on the macroporous support surface. EDS analysis proved that a significant amount of palladium was immobilized binds to the active sites on the interior surface of the particles as well as on the exterior. The higher amount of Pd sorption was observed for PGME 20/14-deta/$PdCl_2$.

The shape of recorded cyclic voltammograms was different for investigated samples. The most pronounced difference was noticed in the potential range of oxide formation and reduction, probably as the consequence of different shape of Pd nanoparticles. The electrochemical response of both investigated samples was similar toward electrooxidation of 4-CP. Nevertheless, the current ratio of formed reversible hydroquinone/benzoquinone couple and oxidation of phenol group was higher at PGME 20/14-deta/$Pd(NO_3)_2$ which might indicate that different 4-CP oxidation paths were favored on investigated electrodes. The probable reason could be the different shape of palladium nanoparticles, i.e. different position of palladium active centers.

Acknowledgment

This work was supported by the Ministry of Education, Science and Technological Development of the Republic of Serbia (Grants no. III43001, III 45001 and III43009).

Reference

[1] L.M. Vracar, D.B. Sepa, A. Damjanovic, Palladium Electrode in Oxygen-Saturated Aqueous-Solutions - Reduction of Oxygen in the Activation-Controlled Region, J. Electrochem. Soc. 133 (1986) 1835–1839.

[2] F.H.B. Lima, J. Zhang, M.H. Shao, K. Sasaki, M.B. Vukmirovic, E.A. Ticianelli, R.R. Adzic, Catalytic activity - d-band center correlation for the O2 Reduction reduction reaction on platinum in alkaline solutions, J. Phys. Chem. C. 111 (2007) 404–410.

[3] A. Hitotsuyanagi, S. Kondo, M. Nakamura, N. Hoshi, Structural effects on the oxygen reduction reaction on n(1 1 1)-(1 0 0) series of Pd, J. Electroanal. Chem. 657 (2011) 123–127.

[4] A. Sarapuu, A. Kasikov, N. Wong, C.A. Lucas, G. Sedghi, R.J. Nichols, K. Tammeveski, Electroreduction of oxygen on gold-supported nanostructured palladium films in acid solutions, Electrochim. Acta. 55 (2010) 6768–6774.

[5] H. Erikson, A. Kasikov, C. Johans, K. Kontturi, K. Tammeveski, A. Sarapuu, Oxygen reduction on Nafion-coated thin-film palladium electrodes, J. Electroanal. Chem. 652 (2011) 1–7.

[6] S.W. Huang, K.G. Neoh, E.T. Kang, H.S. Han, K.L. Tan, Palladium-containing polyaniline and polypyrrole microparticles, J. Mater. Chem. 8 (1998) 1743–1748.

[7] S. Kidambi, M.L. Bruening, Multilayered polyelectrolyte films containing palladium nanoparticles: Synthesis, characterization, and application in selective hydrogenation, Chem. Mater. 17 (2005) 301–307.

[8] S. Thiagarajan, R.F. Yang, S.M. Chen, Palladium particles based nano films; electrochemical fabrication, characterization and applications, Int. J. Electrochem. Sci. 6 (2011) 4537–4552.

[9] E. Hariprasad, T.P. Radhakrishnan, Palladium nanoparticle-embedded polymer thin film “dip catalyst” for Suzuki-Miyaura reaction, ACS Catal. 2 (2012) 1179–1186.

[10] H. Yamato, T. Koshiba, M. Ohwa, W. Wernet, M. Matsumura, A new method for dispersing palladium microparticles in conducting polymer films and its application to biosensors, Synth. Met. 87 (1997) 231–236.

[11] A.B. Nastasović, B.M. Ekmeščić, Z.P. Sandić, D. V. Ranđelović, M. Mozetič, A. Vesel, A.E. Onjia, Mechanism of Cu(II), Cd(II) and Pb(II) ions sorption from aqueous solutions by macroporous poly(glycidyl methacrylate-co-ethylene glycol dimethacrylate), Appl. Surf. Sci. 385 (2016) 605–615.

[12] A. Nastasović, Z. Sandić, L. Suručić, D. Maksin, D. Jakovljević, A. Onjia, Kinetics of hexavalent chromium sorption on amino-functionalized macroporous glycidyl methacrylate copolymer, J. Hazard. Mater. 171 (2009) 153–159.

[13] D.D. Maksin, A.B. Nastasović, A.D. Milutinović-Nikolić, L.T. Suručić, Z.P. Sandić, R. V. Hercigonja, A.E. Onjia, Equilibrium and kinetics study on hexavalent chromium adsorption onto diethylene triamine grafted glycidyl methacrylate based copolymers, J. Hazard. Mater. 209–210 (2012) 99–110.

[14] B.M. Ekmeščić, D.D. Maksin, J.P. Marković, Z.M. Vuković, R. V. Hercigonja, A.B. Nastasović, A.E. Onjia, Recovery of molybdenum oxyanions using macroporous copolymer grafted with diethylenetriamine, Arab. J. Chem. (2015). doi:10.1016/j.arabjc.2015.11.010.

[15] D.D. Maksin, R. V. Hercigonja, M.Ž. Lazarević, M.J. Žunić, A.B. Nastasovic, Modeling of kinetics of pertechnetate removal by amino-functionalized glycidyl methacrylate copolymer, Polym. Bull. 68 (2012) 507–528.

[16] E. Guibal, C. Milot, J.M. Tobin, Metal-Anion Sorption by Chitosan Beads: Equilibrium and Kinetic Studies, Ind. Eng. Chem. Res. 37 (1998) 1454–1463.

[17] M.S. Ureta-Zañartu, M.L. Mora, M.C. Diez, C. Berríos, J. Ojeda, C. Gutiérrez, Chlorophenol electrooxidation on iron oxide-covered aluminosilicates deposited on glassy carbon, J. Appl. Electrochem. 32 (2002) 1211–1218.

[18] C. Berríos, R. Arce, M.C. Rezende, M.S. Ureta-Zañartu, C. Gutiérrez, Electrooxidation of chlorophenols at a glassy carbon electrode in a pH 11 buffer, Electrochim. Acta. 53 (2008) 2768–2775.

[19] F. Fernández, C. Berríos, E. Garrido-Ramírez, N. Escalona, C. Gutiérrez, M.S. Ureta-Zañartu, Electrooxidation of 2-chlorophenol and 2,4,6-chlorophenol on glassy carbon electrodes modified with graphite–zeolite mixtures, J. Appl. Electrochem. 44 (2014) 1295–1306.

[20] M. Tian, B.E. Conway, Phenomenology of oscillatory electro-oxidation of formic acid at Pd: Role of surface oxide films studied by voltammetry, impedance spectroscopy and nanogravimetry, J. Electroanal. Chem. 581 (2005) 176–189.

[21] T. Takamura, Y. Sato, Specular reflectivity studies of the adsorption and the oxidation of methanol on palladium in an alkaline solution, Electrochim. Acta. 19 (1974) 63–68.

[22] R.M. Souto, J.L. Rodríguez, L. Fernández-Mérida, E. Pastor, Electrochemical reactions of benzoic acid on platinum and palladium studied by DEMS. Comparison

with benzyl alcohol, J. Electroanal. Chem. 494 (2000) 127–135.

[23] M.I. Manzanares, A.G. Pavese, V.M. Solis, Comparative investigation of formic acid and formaldehyde electro-oxidation on palladium in acidic medium. Effect of surface oxides, J. Electroanal. Chem. 310 (1991) 159–167.

[24] S.M. Jovanovic, A. Nastasović, N.N. Jovanovic, K. Jeremic, Targeted Porous Structure of Macroporous Copolymers Based on Glycidyl Methacrylate, Mater. Sci. Forum. 214 (1996) 155–162.

[25] L. Malović, A. Nastasović, Z. Sandić, J. Marković, D. Đorđević, Z. Vuković, Surface modification of macroporous glycidyl methacrylate based copolymers for selective sorption of heavy metals, J. Mater. Sci. 42 (2007) 3326–3337.

[26] L. D'Souza, P. Devi, M.P. Divya Shridhar, C.G. Naik, Use of Fourier Transform Infrared (FTIR) spectroscopy to study cadmium-induced changes in Padina tetrastromatica (Hauck), Anal. Chem. Insights. 3 (2008) 135–143.

[27] K. Golcuk, A. Altun, M. Kumru, Thermal studies and vibrational analyses of m-methylaniline complexes of Zn(II), Cd(II) and Hg(II) bromides, Spectrochim. Acta. 59 (2003) 1841–1847.

[28] J.R. Durig, D.W. Wertz, Spectroscopic Review of the Normal Vibrations of Metal Complexes with Nitrogen-Containing Ligands, Appl. Spectrosc. 22 (1968) 627–633.

[29] P.A. Webb, C. Orr, Analytical Methods in Fine Particle Technology, Micromeritics Instrument Corp., Norcross, Georgia, United States, 1997.

[30] D. Horák, J. Labský, J. Pilař, M. Bleha, Z. Pelzbauer, F. Švec, The effect of polymeric porogen on the properties of macroporous poly(glycidyl methacrylate-co-ethylene dimethacrylate), Polymer (Guildf). 34 (1993) 3481–3489.

[31] N. Hoshi, M. Kuroda, Y. Hori, Voltammograms of stepped and kinked stepped surfaces of palladium: Pd(S)-[n(111)x(100)] and Pd(S)-[n(100)x(110)], J. Electroanal. Chem. 521 (2002) 155–160.

[32] J.J. Salvador-Pascual, S. Citalán-Cigarroa, O. Solorza-Feria, Kinetics of oxygen reduction reaction on nanosized Pd electrocatalyst in acid media, J. Power Sources. 172 (2007) 229–234.

[33] R. Hoyer, L.A. Kibler, D.M. Kolb, The initial stages of palladium deposition onto Pt(1 1 1), Electrochim. Acta. 49 (2003) 63–72.

[34] M. Grdeń, M. Łukaszewski, G. Jerkiewicz, A. Czerwiński, Electrochemical behaviour of palladium electrode: Oxidation, electrodissolution and ionic adsorption,

Electrochim. Acta. 53 (2008) 7583–7598.

[35] C.C. Hu, T.C. Wen, Voltammetric investigation of palladium oxides-I: Their formation/reduction in NaOH, Electrochim. Acta. 40 (1995) 495–503.

[36] F.J. Vidal-Iglesias, A. López-Cudero, J. Solla-Gullón, A. Aldaz, J.M. Feliu, Pd-Modified Shape-Controlled Pt Nanoparticles Towards Formic Acid Electrooxidation, Electrocatalysis. 3 (2012) 313–323.

[37] C.S. Kim, K.S. Yoo, Synthesis of Pd particles with various shapes by ionic liquids for HFP hydrogenation catalyst, Res. Chem. Intermed. 40 (2014) 2471–2476.

[38] S. Kondo, M. Nakamura, N. Maki, N. Hoshi, Active Sites for the Oxygen Reduction Reaction on the Low and High Index Planes of Palladium, J. Phys. Chem. C. 113 (2009) 12625–12628.

Figure captions

Fig. 1. FTIR spectra of the (a) PGME 20/14-deta, (b) PGME 20/14-deta/$PdCl_2$ and (c) PGME 20/14-deta/$Pd(NO_3)_2$.

Fig. 2. Cumulative and differential pore size distribution curves for PGME 20/14-deta (a, b) and for PGME 20/14-deta/$Pd(NO_3)_2$ (c, d), respectively.

Fig. 3. SEM microphotographs: PGME 20/14-deta beads (a), particle surface (b), cross-section (c), PGME 20/14-deta/$Pd(NO_3)_2$ beads (d), particle surface (e), cross-section (f), PGME 20/14-deta/$PdCl_2$ beads (g), particle surface (h) and cross-section (i).

Fig. 4. Qualitative SEM-EDS analyses of the features on the surface of PGME 20/14-deta/$Pd(NO_3)_2$ and PGME 20/14-deta/$PdCl_2$. The gray area is the surface of polymer (spectra A) while brighter areas are the palladium-rich phase (spectra B).

Fig. 5. Cyclic voltammograms of PGME 20/14-deta/$PdCl_2$ (solid line and PGME 20/14-deta/$Pd(NO_3)_2$ (dashed line) in 0.1 M H_2SO_4 recorded at scan rate 10 mVs^{-1}. Inset shows enlarged view of cyclovoltammograms.

Fig. 6. Consecutive cyclic voltammograms for different anodic limits recorded in 0.1 M H_2SO_4 at scan rate of 50 mVs^{-1} for a) PGME 20/14-deta/$PdCl_2$ and b) PGME 20/14-deta/$Pd(NO_3)_2$. Inserted pictures represent repetitive cyclovoltammograms 1^{st}, 2^{nd}, 4^{th}, 6^{th}, 10^{th}.

Fig. 7. Consecutive cyclic voltammograms in 5 mM 4-CP + 0.1 M H_2SO_4 recorded at scan rate of 50 mVs^{-1} at: a) PGME 20/14-deta/$PdCl_2$ and b) PGME 20/14-deta/$Pd(NO_3)_2$ previously cycled in 0.1 M H_2SO_4 free of 4-CP. Cyclic voltammograms recorded in 4-CP free solution are also presented.

Fig. 8. Consecutive cyclic voltammograms in 5 mM 4-CP + 0.1 M H_2SO_4 recorded at scan rate of 50 mVs^{-1} at a) PGME 20/14-deta/$PdCl_2$ and b) PGME 20/14-deta/$Pd(NO_3)_2$ without previous conditioning in 0.1 M H_2SO_4 free of 4-CP.

Fig. 9. Mass-transfer corrected Tafel slopes for 4-CP oxidation on PGME 20/14-deta/$PdCl_2$ and PGME 20/14-deta/$Pd(NO_3)_2$ a) with and b) without previous cycling in 4-CP free 0.1 M H_2SO_4.

Table 1 The porosity parameters of the amino-functionalized PGME sample and samples with immobilized Pd(II) ions.

Property	PGME 20/14-deta	PGME 20/14-deta/$PdCl_2$	PGME 20/14-deta/$Pd(NO_3)_2$
$S_{s,Hg}$, $m^2\ g^{-1}$	47	35	32
V_S, $cm^3\ g^{-1}$	0.92	1.05	1.02
$D_{V/2}$, nm	140	172	164

Table 2 Results of SEM-EDS analysis of particle surface and cross-section of PGME 20/14-deta, PGME 20/14-deta/$PdCl_2$ and PGME 20/14-deta/$Pd(NO_3)_2$.

	Particle surface					
Element	**PGME 20/14-deta**		**PGME 20/14-deta/$PdCl_2$**		**PGME 20/14-deta/$Pd(NO_3)_2$**	
	Mass %	**Atomic %**	**Mass %**	**Atomic %**	**Mass %**	**Atomic %**
C-K	70.74	74.82	60.75	76.02	63.02	72.95
O-K	12.01	9.53	11.33	10.64	21.03	18.28
N-K	17.26	15.65	7.86	8.43	7.75	7.70
Cl-K	–	–	7.30	3.09	–	–
Pd-L	–	–	12.77	1.80	8.20	1.07
	Particle cross-section					
Element	**PGME 20/14-deta**		**PGME 20/14-deta/$PdCl_2$**		**PGME 20/14-deta/$Pd(NO_3)_2$**	
	Mass %	**Atomic %**	**Mass %**	**Atomic %**	**Mass %**	**Atomic %**
C-K	67.47	72.11	60.59	75.05	67.07	74.78
N-K	15.61	14.31	15.20	14.13	21.89	18.32
O-K	16.92	13.58	5.83	6.20	6.64	6.35
Cl-K	–		7.32	3.07	–	–
Pd-L	–		11.06	1.55	4.40	0.55

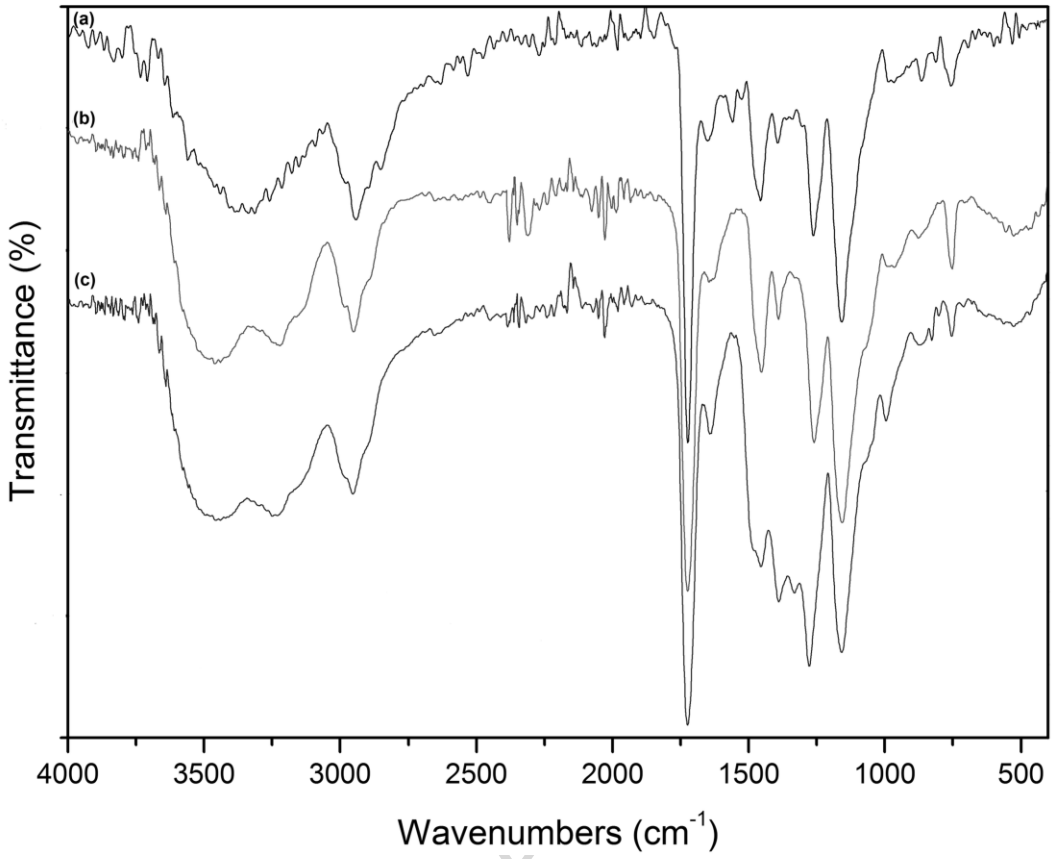

Figure 1

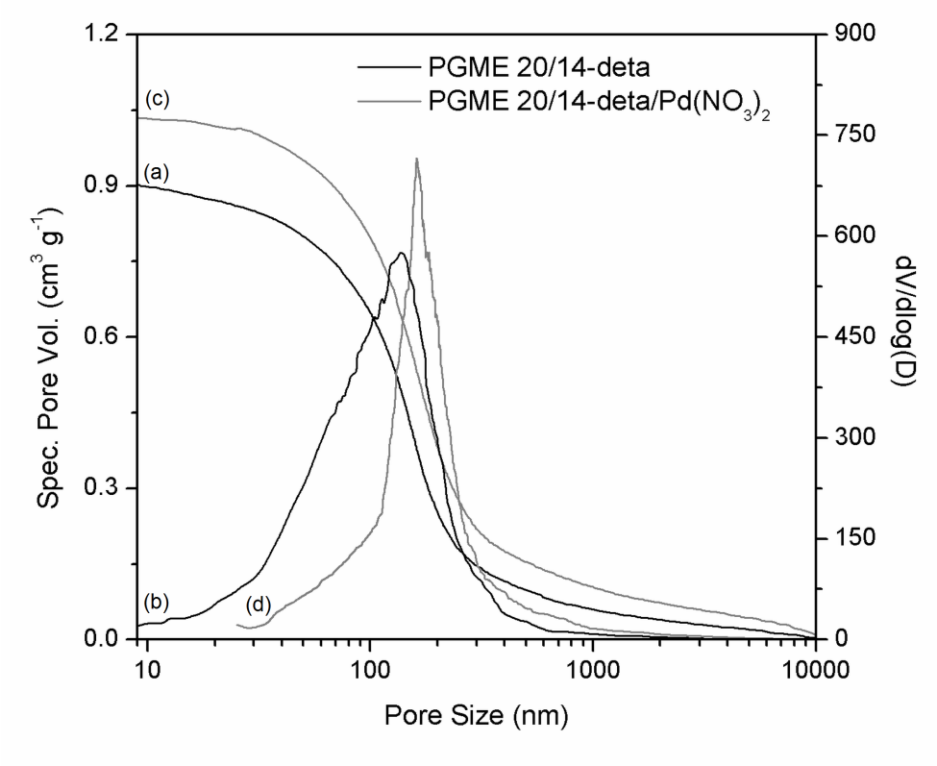

Figure 2

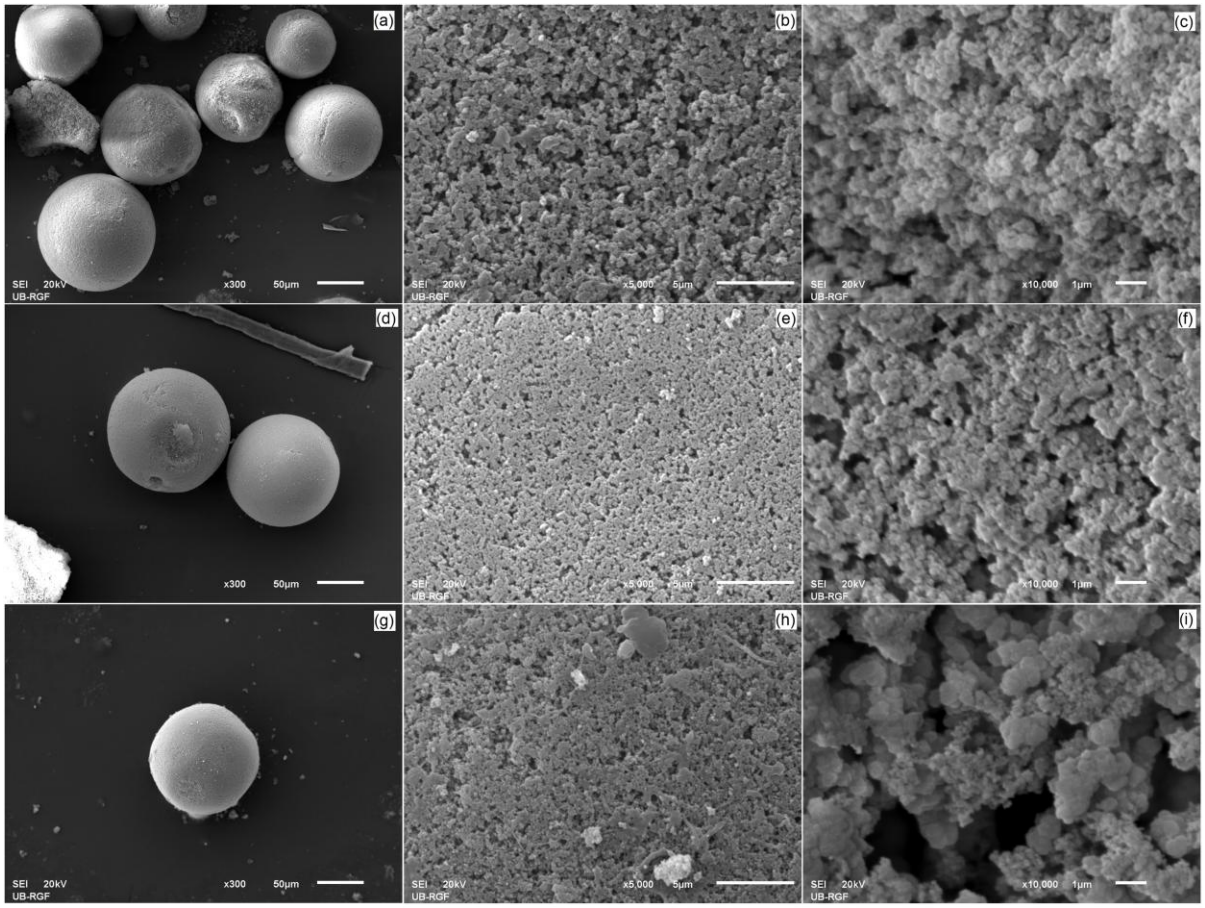

Figure 3

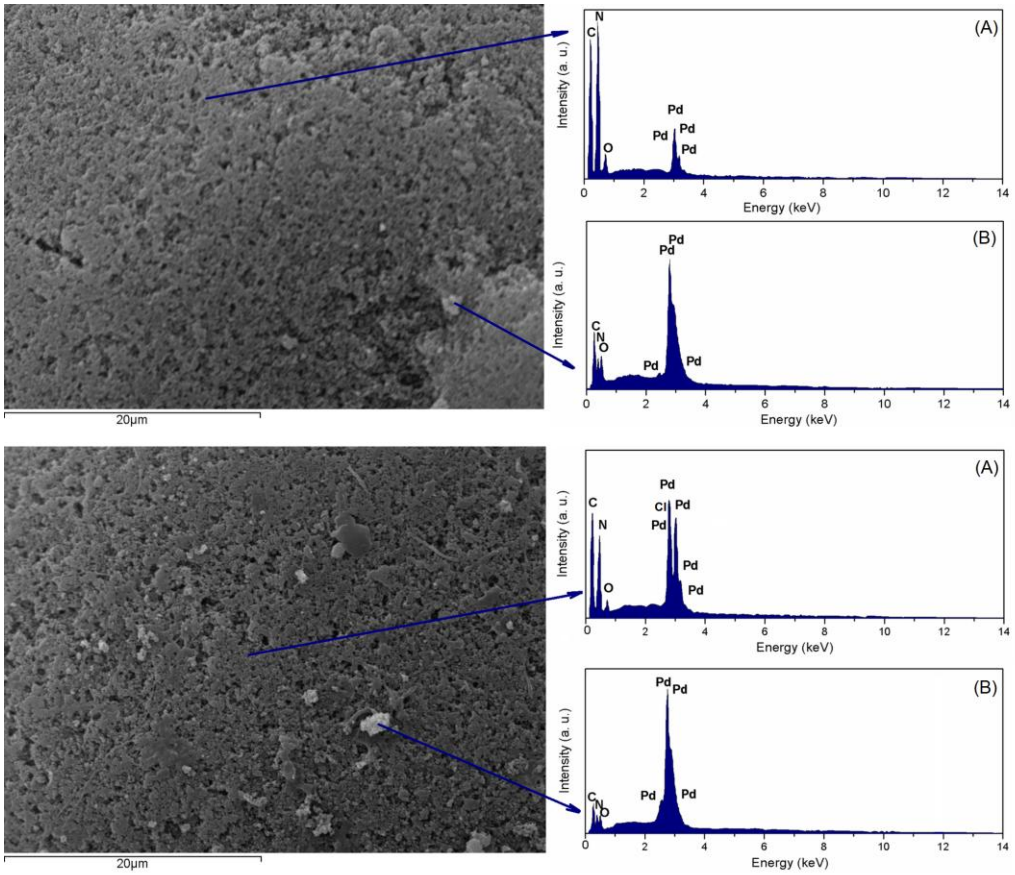

Figure 4

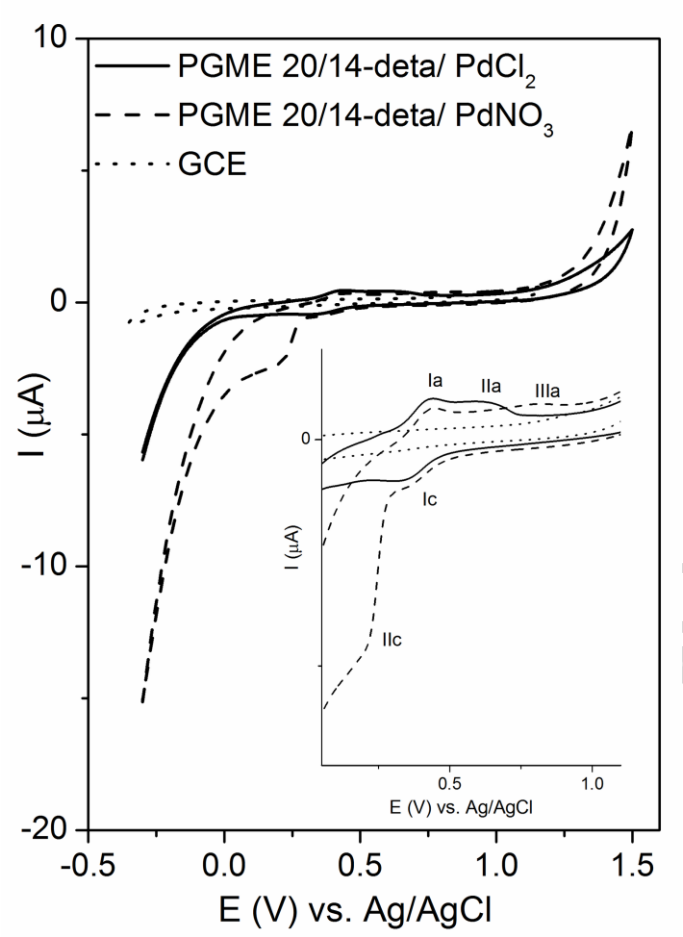

Figure 5

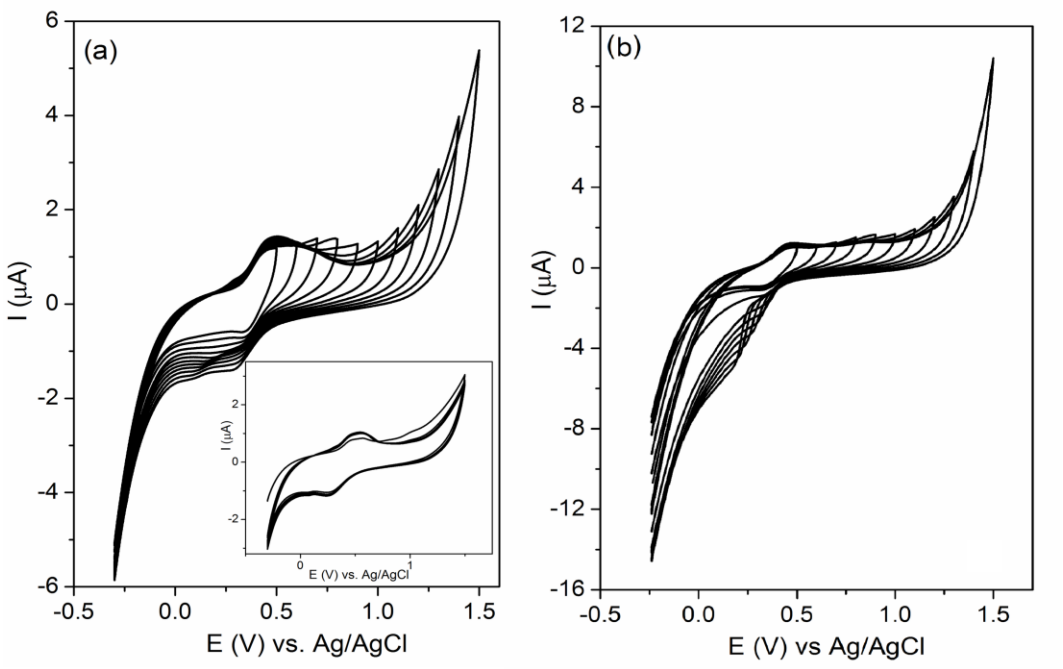

Figure 6

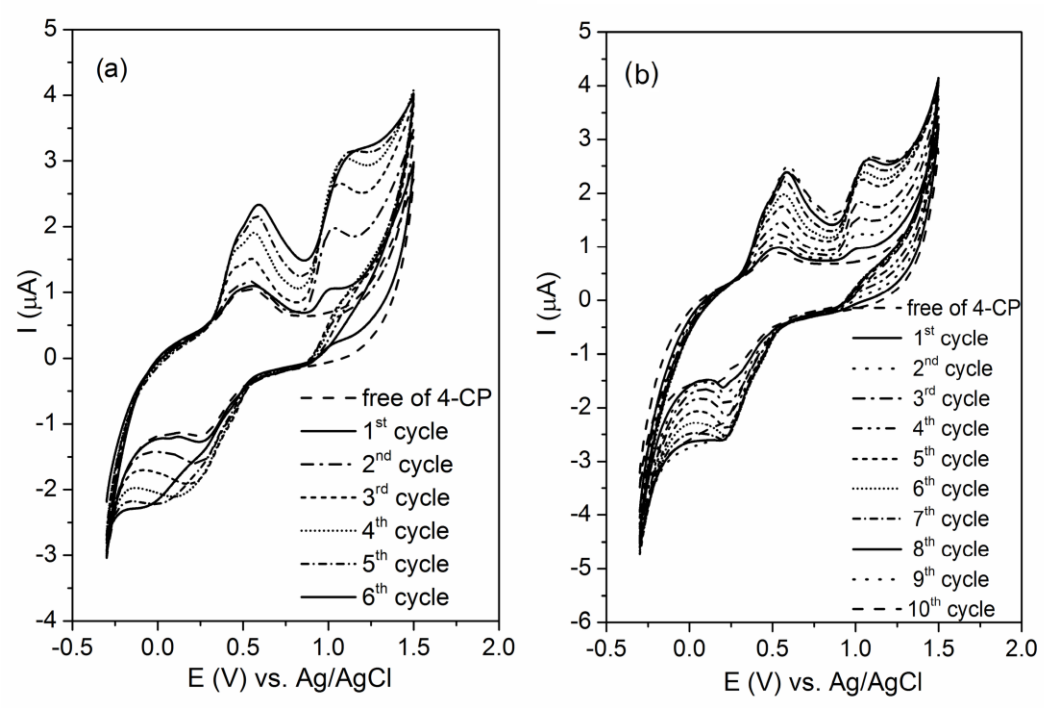

Figure 7

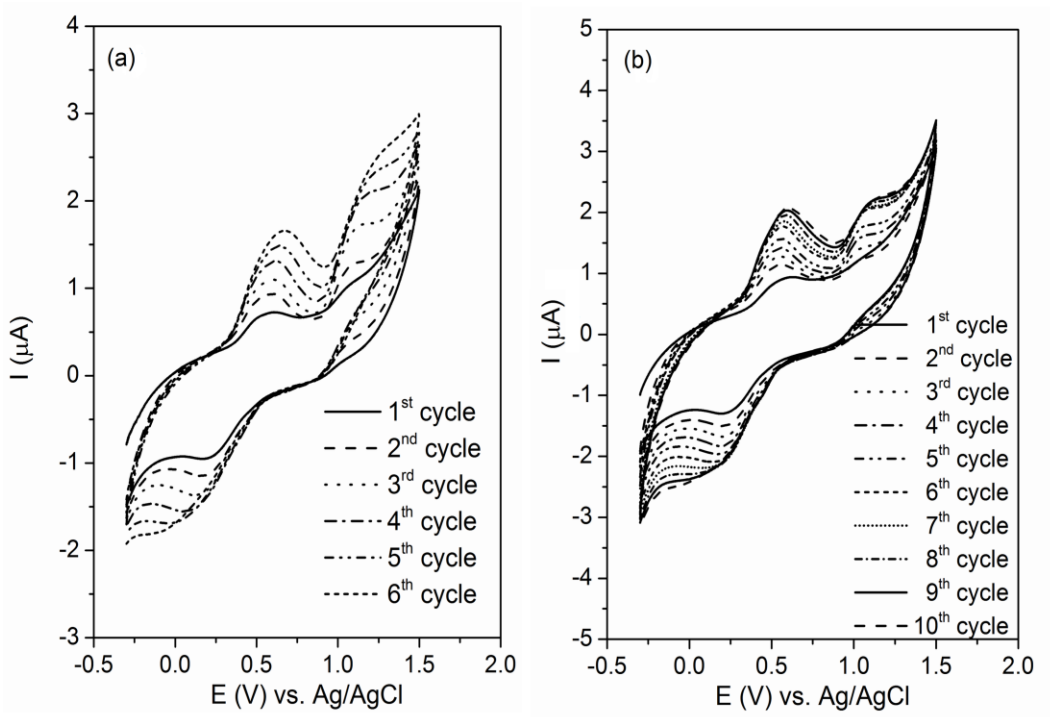

Figure 8

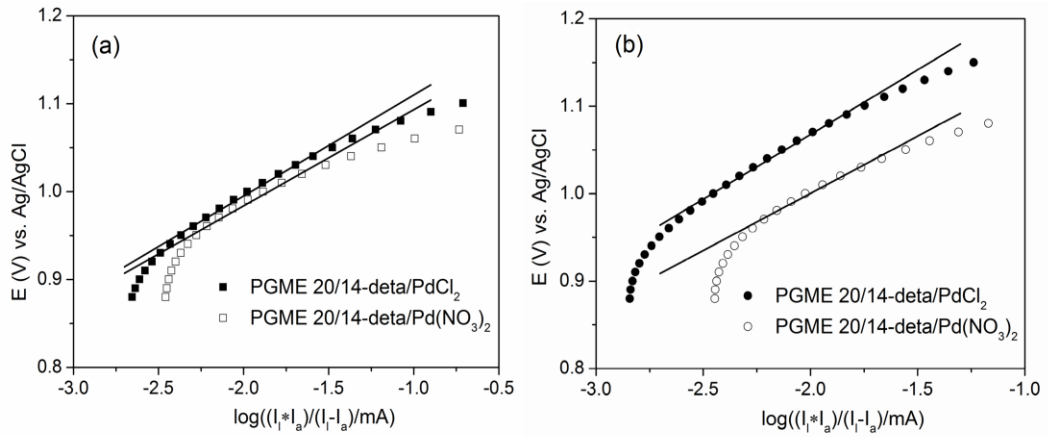

Figure 9

Highlights

- Macroporous copolymer synthesized by suspension copolymerization was amino-functionalized.
- Pd(II) ions were immobilized onto copolymer from chloride and nitrate solutions.
- Pd(II) ions were deposited on the macroporous support as discrete bright aggregates
- The different shape of Pd nanoparticles gave different voltammograms.
- 4-CP oxidation paths were different for different shape of palladium nanoparticles.